JOURNAL OF MATERIALS SCIENCE 31 (1996) 5281–5298

Review
Silicon nitride crystal structure and observations of lattice defects

CHONG-MIN WANG*, XIAOQING PAN, M. RÜHLE
Max-Planck-Institut für Metallforschung, Institut für Werkstoffwinssenschaft, See Str. 92, D-70174, Stuttgart, Germany

F. L. RILEY
School of Materials, The University of Leeds, Leeds LS2 9JT, UK

M. MITOMO
National Institute for Research in Inorganic Materials, Namiki 1-1, Tsukuba, Ibaraki 305, Japan

In view of the considerable progress that has been made over the last 40 years on the microstructural design of silicon nitride and related materials of tailored properties for specific applications, a clear review of the current understanding of the crystal structure and crystal chemistry of silicon nitride is timely. The crystal structures, crystal chemistry, and lattice defect nature of silicon nitride are critically reviewed and discussed, with emphasis placed firstly on the structural nature of α-silicon nitride (whether it is a pure silicon nitride, or should better be regarded as an oxynitride); and secondly on the space group of β-silicon nitride (whether it is $P6_3/m$ or $P6_3$). In conjunction with recent observations of vacancy clusters in α-silicon nitride, a comprehensive view compatible with all the experimental facts with respect to the structural nature of α-silicon nitride is tentatively presented.

1. Purpose and scope of the review

The development of silicon nitride (because of the uncertainty of the stoichiometry, throughout the text we normally use "silicon nitride", but in the case of an assured stoichiometric composition, the formula "Si_3N_4" is used) as a structural engineering material has spanned more than 40 years [1–3]. In the earlier days, research concentrated on crystal structures and phase relationships [4–10]. It has generally been accepted that (a) there are two phases, α-silicon nitride with trigonal symmetry, and β-silicon nitride with hexagonal symmetry, (b) the α- to β-silicon nitride phase transformation occurs above 1400 °C in the presence of a liquid phase through a solution re-precipitation process, or above 1600 °C by a vapour-phase process, and (c) the Si–N bond is approximately 70% covalent and 30% ionic. However, accompanying the development of silicon nitride-based materials, two issues arose. The first concerned the space group of β-silicon nitride: whether it was the centrosymmetric space group, $P6_3/m$, or the non-centrosymmetric, $P6_3$ [6, 7, 11–14]. The second concerned the structural nature of α-silicon nitride: whether it was a pure nitride [15–22] or whether it should better be regarded as an oxynitride with structural oxygen and vacant lattice or interstitial sites [8, 9, 23–27].

For a period of time, experimental effort was directed at resolving these questions. Unfortunately, before any firm conclusions had been reached, interest in these more fundamental aspects was then, to a large extent, replaced by the practical need to develop materials meeting the requirements for engineering applications at high temperature. Research and development activity quickly moved to, and have since been maintained in, aspects of microstructural and compositional design, such as optimization of processing and the choice of densification aids, control of grain growth, characterization of grain-boundary phases, and microstructure–property relationships [28–31]. As a consequence of this effort, silicon nitride-based materials have now reached a stage of microstructural maturity and refinement not matched by many ceramic materials, and with properties tailored to satisfy specific high-temperature or high-load applications [2, 32–34]. However, questions concerning the basic nature of silicon nitride have persisted and cause uncertainty, as reflected in

* *Present address*: National Institute for Reserach in Inorganic Materials, Namiki 1-1, Tsukuba, Ibaraki 305, Japan.

0022–2461

literature citations and in the treatment of crystal structure-related problems [35–37].

A number of aspects provided motivation for the present review. Firstly, although crystal-structure data, and information about lattice defects in silicon nitride, have been reported widely, a detailed review of this subject does not exist. Secondly, information is now being gathered to show that the uncertainties regarding the crystal structure of silicon nitride can be resolved. Lastly, and more importantly, recent direct observations of high densities of lattice defects in α-silicon nitride grains and powder particles [38–42] and the development of intragranular nano-structures [28, 43, 44] have revived interest in the more general question of the defect nature of the α-silicon nitride crystal lattice, its capacity to accommodate localized structural defects, and the nucleation and growth of second phases within the lattice. It is considered that an overall view, incorporating recent progress, will facilitate advances of this subject, and allow areas for further study to be more clearly identified. The hypothesis that α-silicon nitride is a defect structure is the reason for combining treatments of the crystal structure and lattice defects in the review.

2. Crystal structure

The earliest crystal structure determinations of α- and β-silicon nitride [5–7] provided "idealized" structures, but it is still instructive to re-examine these idealized structural models to obtain a better insight into the actual structures, and especially a better understanding of the geometric relationship between α- and β-silicon nitride. Accordingly, we present first the idealized structures, and then some important predictions developed on the basis of building "macro" models of the α- and β-silicon nitride using rigid balls and rods with the idealized structural parameters. Finally, the experimentally measured structural parameters are summarized, and current uncertainties are discussed in detail.

2.1. General description of the crystal structures

After publication of preliminary structural data [5], Hardie and Jack [6], and Popper and Ruddlesden [7], provided the first complete determination of the α- and β-silicon nitride structures through presenting an "idealized" structural model with the parameters listed in Tables I and II for α-Si_3N_4 and β-Si_3N_4, respectively. In both forms the basic building unit is the silicon–nitrogen tetrahedron in which a silicon atom lies at the centre of a tetrahedron, and four nitrogen atoms at each corner (Fig. 1). The SiN_4 tetrahedra are joined by sharing corners in such a way that each nitrogen is common to three tetrahedra: thus each silicon atom has four nitrogen atoms as nearest neighbours, and each nitrogen has three silicon atoms as nearest neighbours.

The structures can also be visualised as the arrangement of puckered Si–N layers. Fig. 2 shows the idealized Si–N layers defined by the parameters given in Tables I and II. The idealized silicon nitride structure can be described as a stacking of the idealized Si–N layers in either an ... ABCDABCD ... sequence for α-Si_3N_4 or ... ABAB ... sequence for the β-Si_3N_4. The AB layer is the same in the α-Si_3N_4 and β-Si_3N_4, and the CD layer in the α-Si_3N_4 is related to the AB layer by a *c*-glide plane.

TABLE I The idealized atomic coordinates for α-Si_3N_4 with space group P31*c* (no. 159) [7]

	x/a	*y/a*	*z/c*
6Si1 in 6(c)	1/12	1/2	3/4
6Si2 in 6(c)	1/4	1/6	1/2
6N1 in 6(c)	2/3	2/3	1/2
6N2 in 6(c)	1/3	1/3	3/4
2N3 in 2(b)	1/3	2/3	3/4
2N4 in 2(a)	0	0	1/2

TABLE II The idealized atomic coordinates for β-Si_3N_4 with space group $P6_3/m$ (no. 176) [7]

	x/a	*y/a*	*z/c*
6Si in 6(h)	3/4	1/6	1/4
6N1 in 6(h)	0	1/3	1/4
2N2 in 2(c)	2/3	1/3	1/4

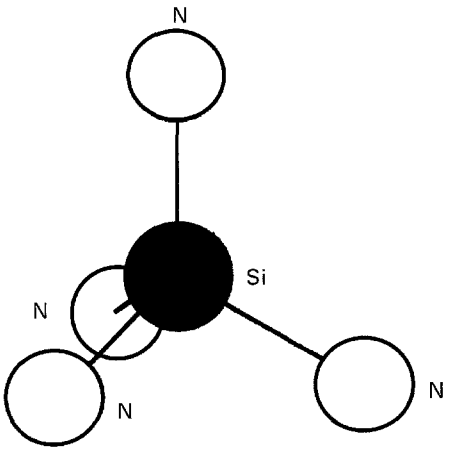

Figure 1 The tetrahedral unit in silicon nitride [29].

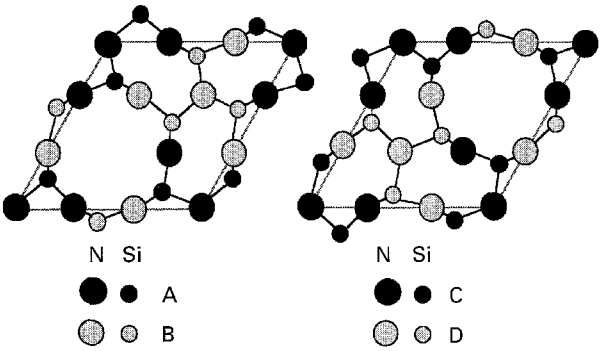

Figure 2 The idealized Si–N layers in α- and β-Si_3N_4 ... ABAB ... for the β-Si_3N_4 structure and ... ABCDABCD ... for the α-Si_3N_4 structure [7, 25].

The idealized α-Si_3N_4 structure has trigonal symmetry of space group P31*c*, within which each unit cell contains four Si_3N_4 units, and $c/a = \frac{2}{5}$. The idealised β-Si_3N_4 structure has hexagonal symmetry with space group $P6_3/m$, and each unit cell contains two Si_3N_4 units with $c/a = \frac{1}{5}$; there are long continuous channels parallel to the hexagonal *c*-axis and centred at $(\frac{2}{3}, \frac{1}{3})$. In α-$Si_3N_4$, the *c*-glide plane relating to the layers CD with AB causes replacement of the continuous channels of the β-Si_3N_4 structure by large closed interstices at $(\frac{1}{3}, \frac{2}{3}, \frac{3}{8})$, and $(\frac{2}{3}, \frac{1}{3}, \frac{7}{8})$. In the idealized forms, the α- and β-Si_3N_4 structures are geometrically related by $a_\alpha = a_\beta$, $c_\alpha = 2c_\beta$.

However, such idealized structures cannot be completely accurate, because they are based on the assumption that the projection of a tetrahedral face on to a plane normal to one of its edges is an equilateral triangle [7]. Subsequent experimental determinations indeed indicated that the structural parameters for both α- and β-silicon nitride deviated from those of the idealized structures. To obtain an insight into the real crystal structures of silicon nitride, Thompson and Pratt [10] and Henderson and Taylor [45] approached these problems macroscopically through constructing models of α- and β-Si_3N_4 from rigid, regular, SiN_4 tetrahedra, based on idealized structure parameters. They realized that to form both α-Si_3N_4 and β-Si_3N_4, different levels of distortion had to be introduced into the regular SiN_4 tetrahedra.

α-Si_3N_4 cannot be built with rigid, regular, tetrahedra. In order to form the α-Si_3N_4 structure the tetrahedra must be distorted and tilted, and all the planar Si_3N groups made slightly pyramidal. From the model, the *c/a* ratio was measured to be 0.715, compared to 0.667 given by the idealized structure.

In β-Si_3N_4 the tetrahedra can be linked with one edge parallel to, and one edge perpendicular to, the (0 0 0 1) plane, with very little distortion of the tetrahedra or Si_3N groups. The main distortion is caused by forcing the Si–Si and N–N distances to be equal in the *c* direction by distortion of the N–Si–N and Si–N–Si angles. In consequence, the $Si_3N(1)$ groups perpendicular to the (0 0 0 1) plane deviate slightly from a planar arrangement. In the model, the *c/a* ratio was measured to be 0.385 for the β-Si_3N_4 compared to 0.333 given by the idealized structure.

It is reasonable to assume that the distortions produced on assembling a ball and rod model are similar to the deviations of the actual crystal structure from the idealized one. Thus β-Si_3N_4 consists of superimposed layers of linked, puckered rings formed by joining six SiN_4 tetrahedra with little strain in bonds and bond angles. α-Si_3N_4 consists of two distorted β-Si_3N_4 layers rotated with respect to each other and joined in the [0 0 0 1] direction. The actual Si–N layers are shown in Fig. 3, which is drawn from the experimentally determined structural data listed in Tables III and IV. Si–N layers in the actual β-Si_3N_4 are almost identical with the ideal configuration (Fig. 2); those of α-Si_3N_4 are considerably distorted, and nitrogen atoms at heights approximately 3/8 and 7/8 are shifted towards the centres of the two respective interstices.

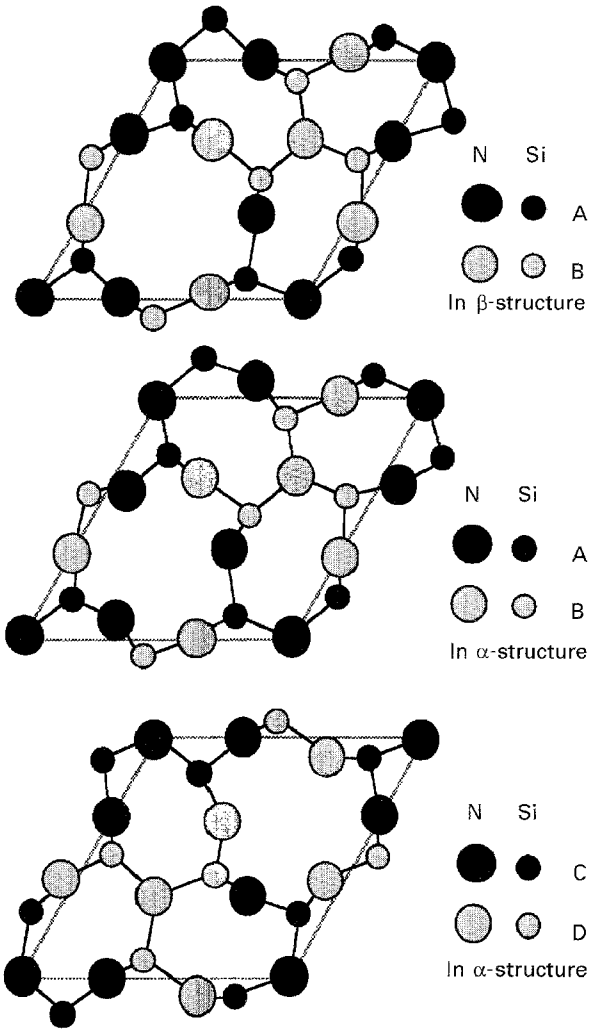

Figure 3 The actual Si–N layers in α- and β-Si_3N_4: ... ABAB ... for the β-Si_3N_4 structure and ... ABCDABCD ... for the α-Si_3N_4 structure [11, 20, 25].

TABLE III The actual atomic coordinates for α-Si_3N_4 with space group P31*c* (no. 159) [20][a]

	x/a	*y/a*	*z/c*
6Si1 in 6(c)	0.0829 (1)	0.5135 (1)	0.6558 (2)
6Si2 in 6(c)	0.2555 (1)	0.1682 (1)	0.4509
6N1 in 6(c)	0.6558 (3)	0.6075 (3)	0.4320 (5)
6N2 in 6(c)	0.3154 (3)	0.3192 (3)	0.6962 (5)
2N3 in 2(b)	0.3333	0.6667	0.5926 (10)
2N4 in 2(a)	0	0	0.4503 (12)

[a] In all tables, the standard deviation is shown as 0.7686 (1) for 0.7686 ± 0.0001.

TABLE IV The actual atomic coordinates for β-Si_3N_4 with space group $P6_3$ (no. 173) [11]

	x/a	*y/a*	*z/c*
6Si in 6(h)	0.7686 (1)	0.1744 (1)	0.2500
6N1 in 6(h)	0.0298 (3)	0.3294 (3)	0.2628 (20)
2N2 in 2(c)	0.6667	0.3333	0.2392 (55)

2.2. α-silicon nitride

2.2.1 Space group

The crystal structure of α-silicon nitride has been determined repeatedly by a large number of

investigators, using a variety of samples ranging from single-crystal to polycrystalline materials synthesized by a wide range of methods of preparation. The results are summarized in Table V. The space group P31*c* is unanimously determined as the correct one for the α-silicon nitride. However, with regard to the crystal structure of α-silicon nitride, two important factual points have to be addressed. The first is the question of oxygen contamination; the second is the lattice distortion because of constraints imposed on the structure by the alternating AB and CD Si–N layers.

2.2.2. Unit-cell dimension

It is obvious that the unit-cell dimensions of α-silicon nitride as determined by different investigators vary widely [46, 47]. Such large differences in the unit-cell dimensions cannot be attributed solely to experimental errors introduced by the different investigators. This can be verified immediately by comparing the distributions of the unit-cell dimensions determined by different investigators for α-silicon nitride and β-silicon nitride as listed in Tables V and VI. For β-silicon nitride, the standard deviation is 0.0005 and 0.0004 nm for the *a* and *c* dimensions, respectively, while for the α-silicon nitride, the corresponding values are 0.0014 and 0.0008 nm. In fact, even with the same investigator using the same method, the unit-cell dimension and density determined on samples prepared by different methods have wide variations, which are well outside any experimental error [28]. α-silicon nitride with a needle morphology prepared

TABLE V Structural data for α-silicon nitride with space group P31*c* (no. 159). Note the calculated density with respect to the nominal oxygen contents

a (nm)	*c* (nm)	*c*/*a*	Density (g cm^{-3})		Oxygen content (wt %)	Sample	Ref.
			Calculated	Measured			
0.7818 (3)	0.5591 (4)	0.715	3.150	–[a]	0.05 (3)	Single crystal	[20]
0.7765 (1)	0.5622 (1)	0.724	3.176	–	–	Single crystal	[15]
0.7766 (10)	0.5615 (8)	0.723	3.178	–	–	Single crystal	[17]
0.7759 (1)	0.5628 (2)	0.725	3.177	3.18	0.1	CVD polycrystal	[52]
0.7758 (5)	0.5623 (5)	0.725	3.180	–	–	Whisker	[46]
0.7754 (2)	0.5625 (3)	0.725	3.182	3.17	0.3	CVD polycrystal	[52]
0.7753 (2)	0.5625 (3)	0.725	3.182	3.17	0.3	CVD polycrystal	[52]
0.77608 (10)	0.56139 (10)	0.723	3.183	–	0.300 (5)	CVD polycrystal	[16]
0.7752 (3)	0.5627 (3)	0.726	3.183	3.18	0.3	CVD polycrystal	[50]
0.7753 (1)	0.5625 (1)	0.726	3.183	–	0.3	CVD polycrystal	[51]
0.7755 (5)	0.5616 (5)	0.725 (1)	3.185	–	–	Powder	[10]
0.7752 (1)	0.5623 (1)	0.725	3.185	3.18	0.6	CVD polycrystal	[50]
0.7752 (2)	0.5623 (2)	0.725	3.185	3.18	0.6	CVD polycrystal	[50]
0.7750 (2)	0.5625 (1)	0.726	3.186	3.17	0.4	CVD polycrystal	[50]
0.7752 (3)	0.5619 (1)	0.725	3.187	–	–	Polycrystal	[47]
0.7751 (2)	0.5622 (2)	0.725	3.187	3.16	0.7	CVD polycrystal	[50]
0.7752 (4)	0.5619 (3)	0.725	3.187	3.16	1.1	CVD polycrystal	[50]
0.7753 (1)	0.5618 (1)	0.725	3.187	–	1.1	CVD polycrystal	[51]
0.7753 (4)	0.5618 (4)	0.725	3.187	3.19	–	Powder	[7]
0.77520 (7)	0.56198 (5)	0.725	3.187	–	1.48[b]	Powder (wool)	[9]
0.77533 (8)	0.56167 (6)	0.724	3.188	3.169 (4)	1.48[b]	Powder (needles)	[9]
0.7748 (1)	0.5617 (1)	0.725	3.192	3.19 (1)	–	Powder	[6]
[c]	[c]						[28]

[a] (–) Not available.
[b] $Si_{11.5}N_{15}O_{0.5}$.
[c] See text for another group of data.

TABLE VI Structural data for β-silicon nitride

a (nm)	*c* (nm)	*c*/*a*	Space group	Density (g cm^{-3})		Sample	Method	Ref.
				Calculated	Measured			
0.7608 (5)	0.2911 (1)	0.3826	$P6_3/m$	3.194	3.192 (2)	Powder	X-ray	[9]
0.7606 (3)	0.2909 (2)	0.3825	$P6_3/m$	3.198	–[a]	Powder	X-ray	[7]
0.7608 (1)	0.2911 (5)	0.3826	$P6_3/m$	3.194	–	Powder	X-ray	[6]
0.7605 (5)	0.2907 (3)	0.3821 (2)	$P6_3/m$	3.201	–	Powder	X-ray	[10]
0.7595 (1)	0.29023 (6)	0.3821	$P6_3$	3.214	–	Single crystal	4-circle diffrac.	[11]
–	–	–	$P6_3/m$	–	–	Single crystal	CBED[b]	[12]
0.7600	0.2900	0.3816	$P6_3$	3.213	–	Single crystal	CBED	[13]

[a] (–) Not available.
[b] CBED stands for convergent beam electron diffraction.

by the reaction of silicon monoxide with nitrogen has a range of measured densities, 3.167–3.171 g cm^{-3} [9]. Following investigation of 26 different α-silicon nitride samples prepared by the reaction of silicon with nitrogen, the reaction of silicon monoxide with nitrogen, and chemical vapour deposition from silicon halides, Thompson observed variations in the unit cell dimensions ranging from 0.774 91–0.775 72 nm for a and from 0.562 64–0.562 21 nm for c (experimental error ± 0.000 05 nm) while the axial ratios c/a are reasonably constant, leading to the conclusion that such a variation of the unit-cell dimension must be due to a variation in compositions, and specifically in the oxygen content [28]. Attempting a better way for addressing the above experimental facts forms the basis for the considerable controversy over the structural nature of α-silicon nitride with respect to the lattice oxygen.

Fig. 4 shows a [0 0 0 1] perspective view of the α-Si_3N_4. There are eight distinct Si–N bonds ranging from 0.1707–0.1779 nm [15] and the average Si–N bond length is 0.1738 nm. The deviations of the nitrogen atoms from the Si_3 planes are 0.0035 and 0.017 nm for N(1) and N(2), and 0.0003 and 0.0350 nm for N(3) and N(4) [11]. Owing to the stacking of alternate layers of AB and CD, there are two closed pockets. The ends of these pockets are formed by single nitrogen atoms. The remainder of the pocket is formed by silicon and nitrogen atoms with bonds lying approximately in the (1 1 $\bar{2}$ 1) planes. The pocket has an equivalent sphere of radius of approximately 0.146 nm. The tunnels connecting the pockets have a minimum radius of 0.07 nm. Consequently, large foreign atoms or molecules could be trapped within the lattice while small ones, such as oxygen, will be able to diffuse rapidly within the lattice (the atomic radius of oxygen is 0.06 nm; the non-bonded radius of oxygen is 0.113 nm; the ionic radius of O^{-2} ranges from 0.135–0.142 nm depending on the coordination numbers).

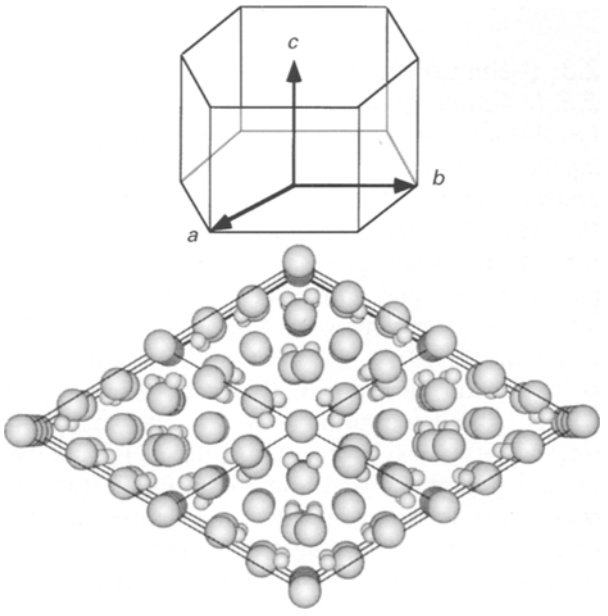

Figure 4 The [0 0 0 1] direction perspective view of α-Si_3N_4. The large spheres are nitrogen, the small silicon. The unit cell is shown by the thick line.

2.2.3. Structural oxygen in α-silicon nitride

Based on structural refinement data of bond lengths and angles, abnormal site occupation numbers, density, and oxygen content, Grieveson and co-workers [8, 9] proposed that α-silicon nitride was an oxynitride with a range of compositions lying between $Si_{11.4}N_{15}O_{0.3}$ and $Si_{11.5}N_{15}O_{0.5}$, and with an oxygen content ranging from 0.90–1.48 wt %. Thus, α-silicon nitride could be regarded as an oxygen- and vacancy-stabilized structure, with oxygen partially replacing nitrogen in the N(1) site, with about 25% nitrogen vacancies in the N(4) site, and with silicon vacancies sufficient to maintain electrical neutrality. This proposition was used to explain the relatively wide variation of densities and unit-cell dimensions observed in the α-silicon nitride. Additional supporting evidence for this claim was provided by thermodynamic studies [23, 24].

Further experimental evidence confirmed that oxygen could indeed dissolve in the α-silicon nitride lattice. Detailed analysis of the oxygen distribution in α-silicon nitride powder show that oxygen exists both as a surface oxide-rich layer, and internally within the particle [26, 27, 48, 49]. However, based on the analysis of oxygen distribution within several fine ceramic powders (~ 100 nm), it is revealed that the majorities of the oxygen exist as a surface oxide layer [49].

There is, in fact, a close relationship between measured oxygen content and the crystal structural parameters. On the basis of a study using CVD polycrystalline α-silicon nitride, Niihara and Hirai [50] and Galasso *et al.* [51] showed that the c-axis unit-cell dimension and the unit-cell volume (and density) increase with decreasing oxygen content, while the a dimension is almost independent of oxygen content. Doubt may be expressed regarding this empirical rule with respect to its generality, as it does not specify the distribution of the oxygen, as a surface oxide layer or dissolved in the lattice. Unit-cell dimensions, and unit-cell volume, as a function of the measured oxygen content, are shown in Figs 5 and 6. Scrutiny of the structural data listed in Table VI shows that the calculated densities obtained with single crystals (ranging from 3.150–3.178 g cm^{-3}), are generally lower than those obtained with polycrystals (3.177–3.192 g cm^{-3}). Single crystals of α-silicon nitride contain lesser amounts of oxygen than the polycrystalline form. This, therefore, coincides with the general trend, that with decreasing oxygen content the unit-cell volume increases (Fig. 6).

However, subsequent structural determinations on materials for which it was unnecessary to assume that α-silicon nitride was anything but the stoichiometric Si_3N_4, cast doubt on the oxynitride hypothesis [15, 17, 19, 20]. Priest *et al.* [16] carried out neutron activation analysis on a single crystal of α-silicon nitride prepared by CVD and found the oxygen content to be 0.3 ± 0.005 wt %, an amount substantially less than the 0.9–1.48 wt % that was assumed to be required for

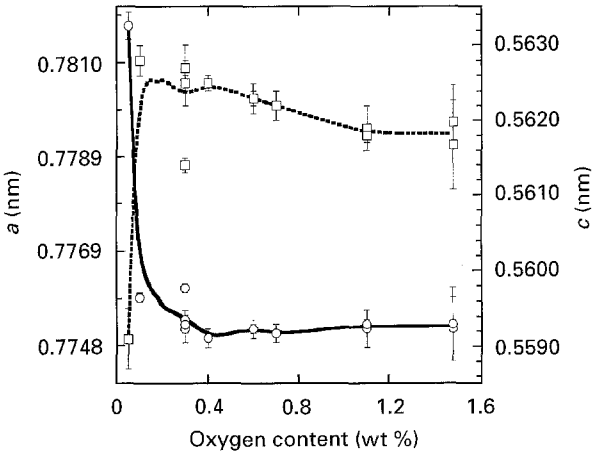

Figure 5 The unit-cell dimensions of α-silicon nitride as a function of the nominal oxygen content. (—○—) *a*, (---□---) *c*.

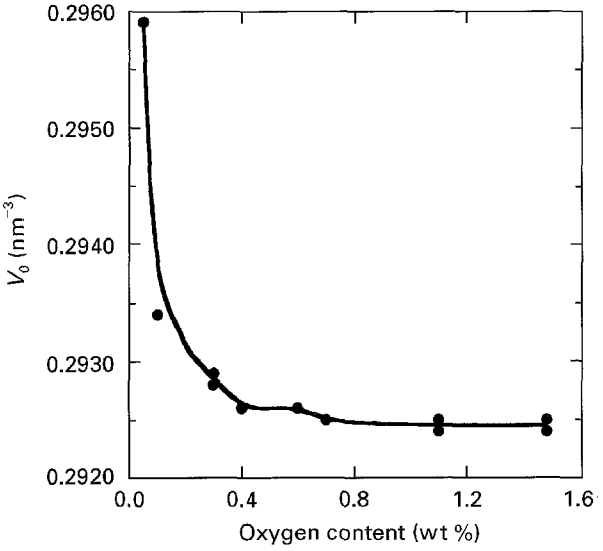

Figure 6 The α-silicon nitride unit-cell volume, V_0, as a function of the nominal oxygen content.

the oxynitride. Edwards *et al.* [18] also analysed various samples of reaction-bonded silicon nitride and found that the oxygen content lay between 0.45 ± 0.05 and 0.61 ± 0.06 wt %, again far too low for Grieveson and co-workers *et al.* oxynitride formula to be correct [8, 9]. Later, Kijima *et al.* [19] measured oxygen contents of 0.05 and 0.09 wt % on α-silicon nitride single crystals. In addition, the structural parameter determination of Kato *et al.* [20] was done on the same crystal known to have a low oxygen content (0.05 wt %) from analytical work. Therefore, on the basis of the combined oxygen analysis and structure determinations, it was established that α-silicon nitride did not necessarily require the level of oxygen suggested by Grieveson and co-workers for structural stabilization.

Following the discovery of the sialon systems it was possible to argue, by analogy with the stabilization of the α′-sialon structure by cations such as Ca^{2+} and Y^{3+}, that the pure α-silicon nitride structure might be stabilized by a lower valence silicon species accommodated in structural interstices [28]. Si^{4+} is too small to be accommodated in interstitial sites and so Si^{3+} was suggested. The corresponding compositions would then be $Si^{3+}_{0.3}Si^{4+}_{11.8}N^{3-}_{16}$ or $Si^{3+}_{0.3}Si^{4+}_{11.8}O^{2-}_{0.5}N^{3-}_{15.5}$ depending on the availability of oxygen for charge compensation. As a consequence of the partial occupation of the interstitial sites, there might be locally structural distortion.

A compromise view on the role of oxygen in α-silicon nitride compatible with all of the above experimental facts, is that α-silicon nitride is able to accommodate variable amounts of oxygen, depending on the availability of the oxygen in the processing environment, although oxygen is not a necessary requirement for the stability of the α-silicon nitride structure. The observed wide variations of density and unit-cell dimension of α-silicon nitride are attributed to the variation of the oxygen content of the α-silicon nitride lattice, resulting from different preparation routes. The lowest limit for oxygen dissolved in the α-silicon nitride lattice is expected to be zero. Such pure and perfect single-crystalline α-Si_3N_4 material must be essentially transparent and colourless, because the optical adsorption edge is about 310 nm [52]. In practice, as oxygen is an inevitable environmental impurity, the purest single-crystalline α-silicon nitride to be reported still contains 0.05 wt % oxygen [19, 20]. This single crystal was colourless, with unit cell dimensions of $a = 0.7818 \pm 0.0003$ nm, $c = 0.5591 \pm 0.0004$ nm and $c/a = 0.715$. It should be pointed out that although the majority of the c/a values for the α-silicon nitride structure listed in Table VI are in the region of 0.725, the lowest value of 0.715 obtained with this single crystal (known to include a low amount of oxygen) is remarkably close to that measured on the macro-model of the α-Si_3N_4 structure (0.715) in which oxygen is, in effect, artificially excluded [10, 20]. Generally, the colour of polycrystalline CVD α-silicon nitride depends on the preparation process, and can be white, purple, brown or black [28].

2.3. β-silicon nitride

2.3.1. Space group

For β-silicon nitride, the only disagreement concerning the structure was the space group: whether it is the centrosymmetric, $P6_3/m$, or the non-centrosymmetric, $P6_3$ (Table VI). In the structure of space group $P6_3/m$, the silicon and nitrogen atoms are located on mirror planes ($z = 1/4$ and $3/4$) normal to the c-axis, as indicated by several powder X-ray diffraction determinations [6, 7, 9, 10, 12], and by a single convergent beam electron diffraction (CBED) determination [12]. On the other hand, using structural refinement with single-crystal X-ray diffraction, Grün [11] noted that the nitrogen atoms were slightly displaced from the mirror planes, implying the non-centrosymmetric space group $P6_3$. Subsequently, in a determination of the space group by the CBED method, Bando [13] observed that the apparent CBED symmetry depended on the thickness of the sample. It was shown that for a thin crystal the space group could be allocated to $P6_3/m$, in agreement with the previous independent

CBED determination [12], while for a thick crystal the lower symmetry of $P6_3$ is revealed. The CBED pattern for a thick crystal shows the real crystal potential related to both silicon and nitrogen atom arrangements, and reveals the true space group as $P6_3$. Bando's observation apparently biases the current debate about the space group of β-silicon nitride in favour of Grün's claim. In principle, if $P6_3/m$ is assumed, all atoms are located in a mirror plane, so that all the $Si_3N(1)$ and $Si_3N(2)$ groups have to be planar. This is not completely true, as proved by actual construction of the ball and rod model structure, which shows that $Si_3N(1)$ groups possess a non-planar configuration. The deviations of N(1) and N(2) from the corresponding Si_3 plane are 0.0048 and 0.0040 nm, respectively. Furthermore, Grün has calculated the lattice energy difference between the centrosymmetric and the non-centrosymmetric structures, and concluded that the non-centrosymmetric structure would be energetically more favoured. Thus it seems reasonable to believe that the space group, $P6_3$, is the correct one for β-silicon nitride.

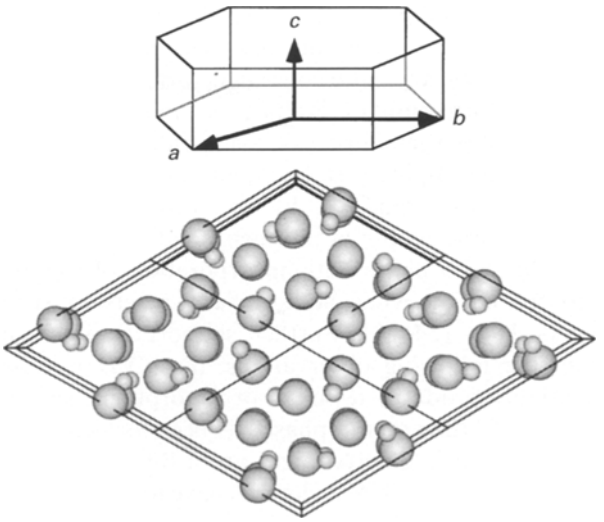

Figure 7 The [0001] direction perspective view of β-Si_3N_4 in which the long continuous channel parallel to [0001] can be seen. Large spheres are nitrogen, the small are silicon. The unit cell is represented by the thick line.

2.3.2. Unit-cell dimension

The large number of investigations of the crystal structure of β-silicon nitride are summarized in Table VI [6, 7, 9, 10–14]. It is apparent that the a and c unit-cell dimensions, c/a, and density, measured by different investigators are in very good agreement.

Fig. 7 shows a [0001] perspective view of β-Si_3N_4. The long continuous channels parallel to the c-axis can be seen. The average Si–N bond length is 0.173 nm (there are four distinct values ranging from 0.1704–0.1767 nm) [10, 11]. Using this value, the continuous channel has an equivalent cylindrical radius of 0.145 nm, which in theory may enable large atoms to diffuse readily through the lattice. The small six-sided space contains a void of radius 0.09 nm.

2.4. The relationship between the α- and β-silicon nitride structures

α-silicon nitride and β-silicon nitride phase relationship may be addressed from two standpoints: firstly the geometric and secondly that of phase stability.

2.4.1. Geometric relationship

The measured unit-cell dimensions of α-silicon nitride and β-silicon nitride have the geometrical relationship $a_\alpha > a_\beta$, $c_\alpha < 2c_\beta$, with $c/a = 0.715$ for α and $c/a = 0.3826$ for β (which are in almost exact coincidence with the values obtained by Thompson and Pratt on the macro structural models [10]). The slight departure from an exact relationship between the unit-cell dimensions of α- and β-silicon nitride is unusual and it is far more common to find polymorphs where the two forms are either structurally unrelated, or are layer modifications (e.g. silicon carbide) where the a values are precisely equal and the c values are in exact integer ratio. However, such a deviation could be superficially explained by the fact that even though α-silicon nitride consists essentially of alternate layers of the β-silicon nitride (AB) and a mirror image of it (CD), the edges of the double layer of the tetrahedra in the α-silicon nitride do not lie exactly parallel to the c axis (as they do for the single-layer β-silicon nitride), but deviate from this with accompanying distortion of their geometric arrangement to allow the individual tetrahedra to become more regular. Such a distortion would reduce the c dimension while increasing the a dimension, resulting in $a_\alpha > a_\beta$, $c_\alpha < 2c_\beta$ [10, 45].

2.4.2. Phase stability

Various opinions exist regarding the α- and β-phase silicon nitride relationship, and these can be classified as follows.

(i) The α-phase is an oxynitride, while the β-phase is a pure silicon nitride; this possibility has been examined in the previous detailed discussion [9, 23, 24, 28, 53].

(ii) The α- and β-phases are the low- and high-temperature modifications, respectively [10, 31]. This view is mostly based on the observations that during nitridation of silicon the proportion of α-phase increases with decreasing temperature, and that above 1400 °C the α-phase transforms to the β-phase [54]. However, if the α- and β-phases are true high- and low-temperature modifications with a specific transformation temperature, it should be possible to observe the reverse transformation, from β-silicon nitride to α-silicon nitride at temperatures below 1400 °C. This has never been observed experimentally (though it may be argued that for such a transformation the mechanism is not available for surmounting the activation barrier at these temperatures).

(iii) The β-phase is the thermodynamically more stable phase at all temperatures, and the development of the two modifications is controlled by the formation mechanism, rather than by thermodynamic considerations [11, 21]. Accordingly, it is argued that

formation of the α-phase is kinetically favoured by the involvement of oxygen and gaseous species such as silicon vapour and SiO, consistent with observations that the formation of α-phase is favoured by the presence of oxygen during silicon nitridation. Formation of the β-phase is favoured by the presence of liquid, as supported by the observation that with the same supply of nitrogen, solid silicon reacts to yield the α-phase with incorporation of oxygen into the lattice, while liquid silicon reacts to yield the β-phase [54–58]. Further support is obtained from the following observations: the CVD process invariably produces α-phase, or amorphous, silicon nitride [28] (however, β-phase has been formed when $TiCl_4$ vapour is incorporated into a $SiCl_4$–NH_3–H_2 reactant system as TiN inclusions have to be necessarily involved for the reason of formation kinetics [59]); oxygen-containing species such as SiO and SiO_xN_x are necessary for the crystallization of amorphous silicon nitride (obtained by imide decomposition or by pyrolysis of polymeric precursor) to α-silicon nitride [60, 61].

Calculations show that the α-phase has a slightly higher free energy than the β-phase: a difference of about 30 kJ mol^{-1} at 25 °C is given by Grün [11], this has been used to demonstrate that transformation from β- to α-phase is, in principle, not possible [11]. The driving force for the transformation from α- to β-phase lies in the higher thermodynamic stability of the β-phase. From the kinetic point of view, this transformation cannot be achieved by a displacive transformation because the two sequences of non-equivalent tetrahedra are distorted with respect to one another around the *c*-axis. A reconstructive process involving the breaking and reconstruction of six Si–N bonds in each unit cell is necessary, together with a change in position of one nitrogen atom and a small displacement of neighbouring atoms. Thus the activation energy will be high while the change in internal energy on transformation is small [10, 11]. The reconstructive transformation can only proceed in the presence of liquid phases (metal silicon or metal silicides) which lower the activation energy for transformation. Studies carried out over the last 30 years show that the α-to β-phase transformation proceeds readily above 1400 °C in the presence of a liquid phase through a solution and re-precipitation process [31, 62–64]. An observation consistent with the necessity for liquid for such a phase transformation is that no transformation was detected in high-purity CVD silicon nitride at 1800 °C [16]. A typical value for the activation energy in the presence of a liquid is about 405 kJ mol^{-1}, that is close to the Si–N bond energy, 435 kJ mol^{-1} [65].

3. Lattice defects in silicon nitride

Vacancies, voids, dislocations, and stacking faults are examples of defects, which are well characterized in metals and alloys. Research on the possible existence of such defects in silicon nitride is limited. Here, vacancies, structural domains, and dislocations are examined [34, 66–69].

3.1. Point defects

3.1.1. α-Silicon nitride

3.1.1.1. Powder particles. Transmission electron microscopy (TEM) observations of several types of α-silicon nitride powder particles prepared by CVD, silicon nitridation, carbothermal reduction of silica, and the imide decomposition process [38–42, 70–73] have shown that high densities of vacancy clusters are a common feature of all forms of α-silicon nitride: the detailed descriptions of the configurations and features of the vacancy clusters, where a vacancy is assumed to be of the Schottky "$V_{Si_3N_4}$" type, are summarized in Table VII. The clusters are of disc shape having a diameter of 15–30 nm. The equivalent overall vacancy concentration appears to range from 10^{-3}–10^{-4} depending on the thermal history of the materials [41]. Vacancy clusters of size large enough to be resolved by TEM are confirmed to be mobile, and at high temperature can either fuse to give further high orders of cluster, or to diffuse out from the lattice, depending on the heat treatment.

Fig. 8 is a low-magnification TEM image of silicon nitride powder produced by silicon nitridation showing particle morphology and size distribution. This powder had been milled giving the mechanically induced lattice strain and associated dislocation networks, as seen in Figs 9 and 10. Rotation of randomly selected particles shows the internal contrast of the characteristic strain fields of the point defects. Unambiguous identification of the nature of the those point defects was impossible because of the size of the larger particles (500 nm), and the disturbance of contrast caused by the attached smaller particles. These

TABLE VII Dislocation loops in α-silicon nitride

Type, nature	Habit plane	Burgers vector	Size (nm)	Ref.
Vacancy, pure edge	$\{\bar{1}\bar{1}21\}$	$\frac{1}{3}\langle 11\bar{2}\bar{3}\rangle$	150	[38,71]
Vacancy, pure edge	$\{11\bar{2}0\}$	$\frac{1}{3}\langle 11\bar{2}0\rangle$	10–30	[40,71]
Vacancy, pure edge	$\{0001\}$	$\langle 0001\rangle$	10–30	[42,71]
Interstitial, mixed	$(12\bar{3}1)$	$\frac{1}{3}\langle 11\bar{2}\bar{3}\rangle$	10–100	[39]

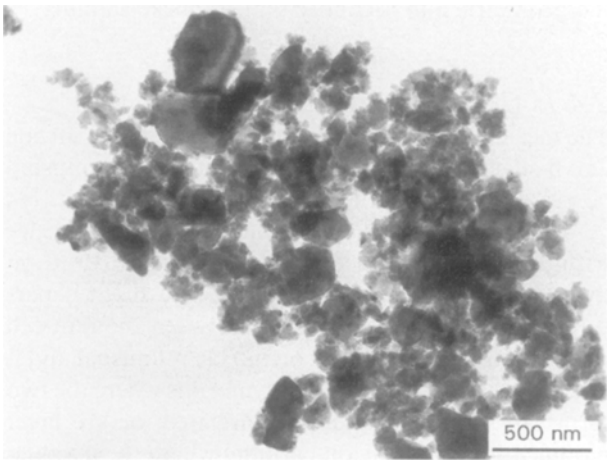

Figure 8 A low-magnification transmission electron micrograph of typical silicon nitride powder obtained by silicon nitridation and milling, showing the wide particle size range.

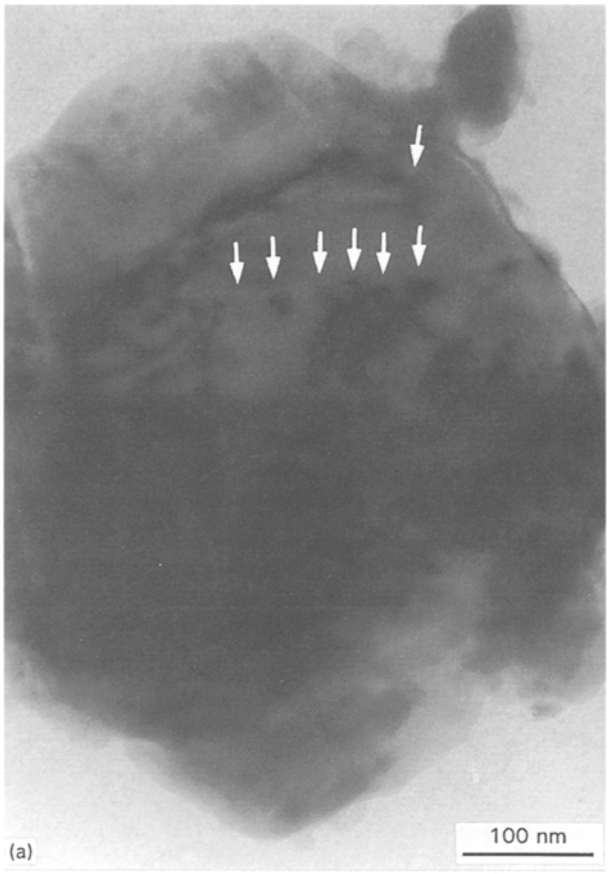

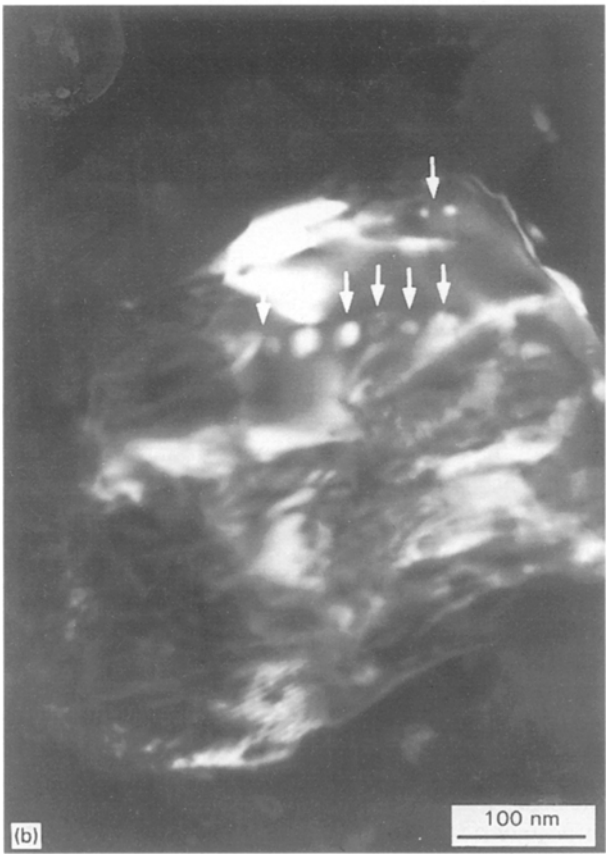

Figure 9 Intragranular spherical features (arrowed) in a selected particle of the powder shown in Fig. 8. (a) Bright field; (b) dark field [41].

features may, however, be vacancy loops on the basis of the observations described below.

Fig. 11a is a low-magnification transmission electron micrograph of an imide-produced silicon nitride

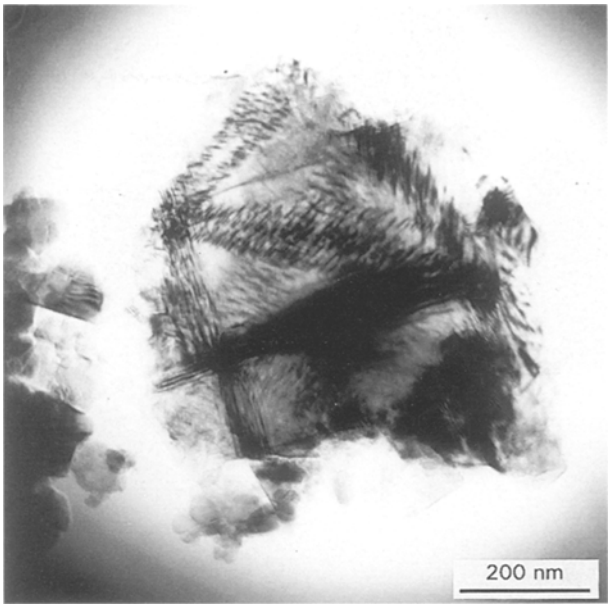

Figure 10 Bragg distinction contour in a selected particle of the powder shown in Fig. 8 indicating that the particle has been severely deformed during post-nitridation milling.

powder. On this scale, the range of image contrast obtainable is narrow because of the particle thickness. The available information is (similar to that obtained from TEM observations of powder particles of the same range of size) thus limited to particle morphology, particle size and size distribution, and possibly the agglomeration state of the particle. The particle size is uniformly distributed around 600 nm, and particles have a very well-defined morphology with a straight grain edge parallel to the c-axis. On preparation of the TEM sample through a suspension drying process, the particles are prone to lie on the supporting carbon film with the c-axis parallel with the film surface, and most of the particles can be easily observed with a zone axis around $[1\,0\,\bar{1}\,0]$. At higher magnification, with a small objective aperture and bright illumination, internal contrast features, similar in appearance to those generated from a precipitate, can be seen within individual particles as shown in Fig. 11b. A statistical analysis in the TEM with 360 particles chosen at random in different areas, showed that 97% had these internal structural features. In addition to the dislocation loops, some particles (43% of the dislocation loops containing particles) concurrently had a stacking fault (arrowed in Fig. 11c). To identify the origin of the loops, the powder was annealed at 1500 and 1750 °C, and cooled slowly to room temperature. After annealing, the dislocation loops remained and a higher proportion of the particles included the stacking fault. Fig. 12 shows a particle in the annealed powder with different zone axis. Generally, at a zone axis $[UVT0]$ such as near $[1\,0\,\bar{1}\,0]$, both the stacking fault and the dislocation loops are edge-on, and for such cases, the stacking fault appears as a line (Fig. 12a); while at a zone axis $[UVTW]$ with $W \neq 0$ such as near $[4\,0\,\bar{4}\,1]$, both the stacking fault and the dislocation loops are inclined; hence the stacking fault is clearly resolved (Fig. 12b). The stacking faults have four features: (i) invariantly

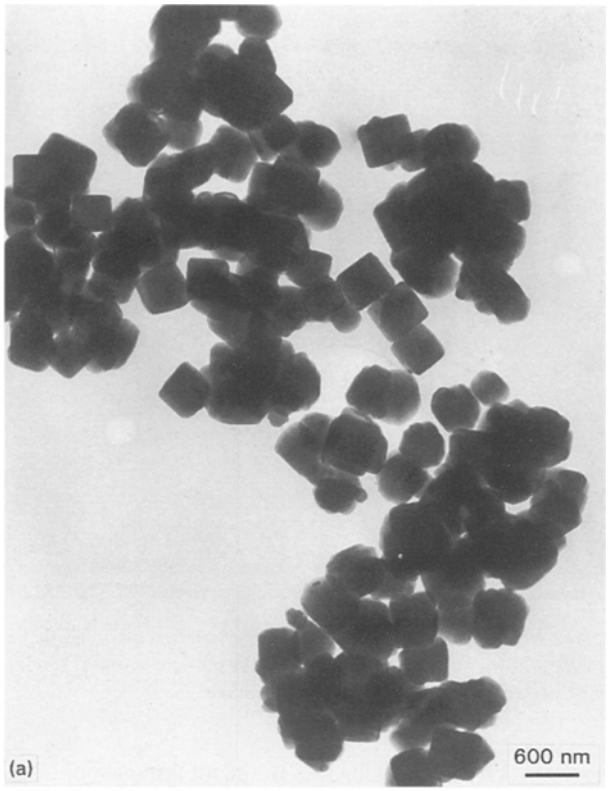

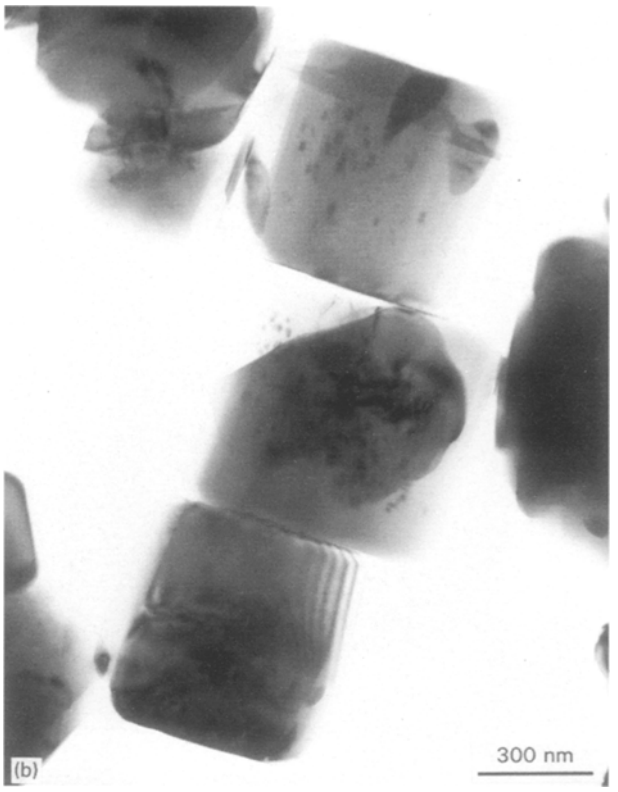

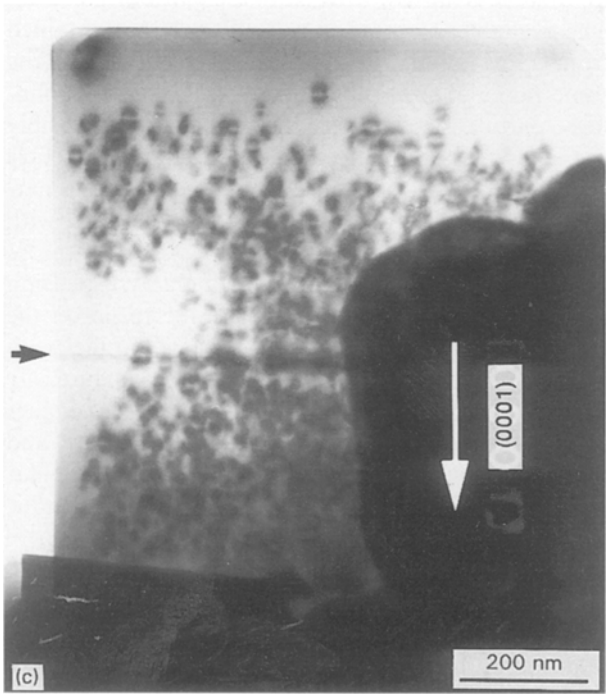

Figure 11 Transmission electron micrographs of as-received UBE-E03 silicon nitride powder particles (produced by imide decomposition and crystallization of the amorphous precursor at 1300–1500 °C). (a) Low magnification, showing the general morphology of the powder particles (bright field); (b) high magnification, three particles in (a) (arrowed) show internal contrast features indicative of vacancy-type dislocation loops; and (c) a large particle observed from zone axes near $[1\,0\,\bar{1}\,0]$, showing a high concentration of dislocation loops and a stacking fault (arrowed).

lying on the (0 0 0 1) plane; (ii) each particle has only one stacking fault; (iii) the stacking fault appears at the centre of the particle with respect to the *c*-axis; (iv) the stacking fault plane intersects the prismatic plane of the particle, indicating that the stacking fault terminates on the free prismatic surface, dividing each particle into two halves along the *c*-axis. Fig. 13 shows dislocation loops and a stacking fault in particles annealed at 1700 °C. The standard inside/outside and ***gb*** (***g*** the operating reflection and ***b*** the Burgers vectors) contrast analysis indicate that this internal feature is invariably a vacancy-type dislocation loop in α-silicon nitride particles. As shown in Figs 11c and 12b, the majority of the loops have a habit plane $\{0\,0\,0\,1\}$ and Burgers vector $(1/n)\langle 0\,0\,0\,1\rangle$ ($n = 1$ or 2) (labelled A), while a small proportion have a habit plane $\{1\,\bar{2}\,1\,1\}$ and Burgers vector $(1/m)\langle \bar{1}\,2\,\bar{1}\,3\rangle$ ($m = 3$ or 9) (labelled B).

From the loop-free zone dimension in as-produced powder particles, a critical particle-size effect has been expected: as-grown particle of size smaller than twice the loop-free zone width should be completely free from dislocation loops. However, this will not be true for fine particles produced by mechanical crushing of a large particle, typical of powder produced by silicon nitridation. More broadly, it is inferred that to produce α-silicon nitride particles free from dislocation loops and vacancy clusters, control of as-grown particle size and cooling rate will be needed to allow vacancies formed at processing temperature to diffuse to boundaries or surfaces.

3.1.1.2. Grains in polycrystalline silicon nitride materials. A number of α-silicon nitride grains in polycrystalline silicon nitride materials prepared by different methods have been observed using high-resolution transmission electron microscopy (HRTEM) along the [0 0 0 1] direction [74]. Localized strain centres

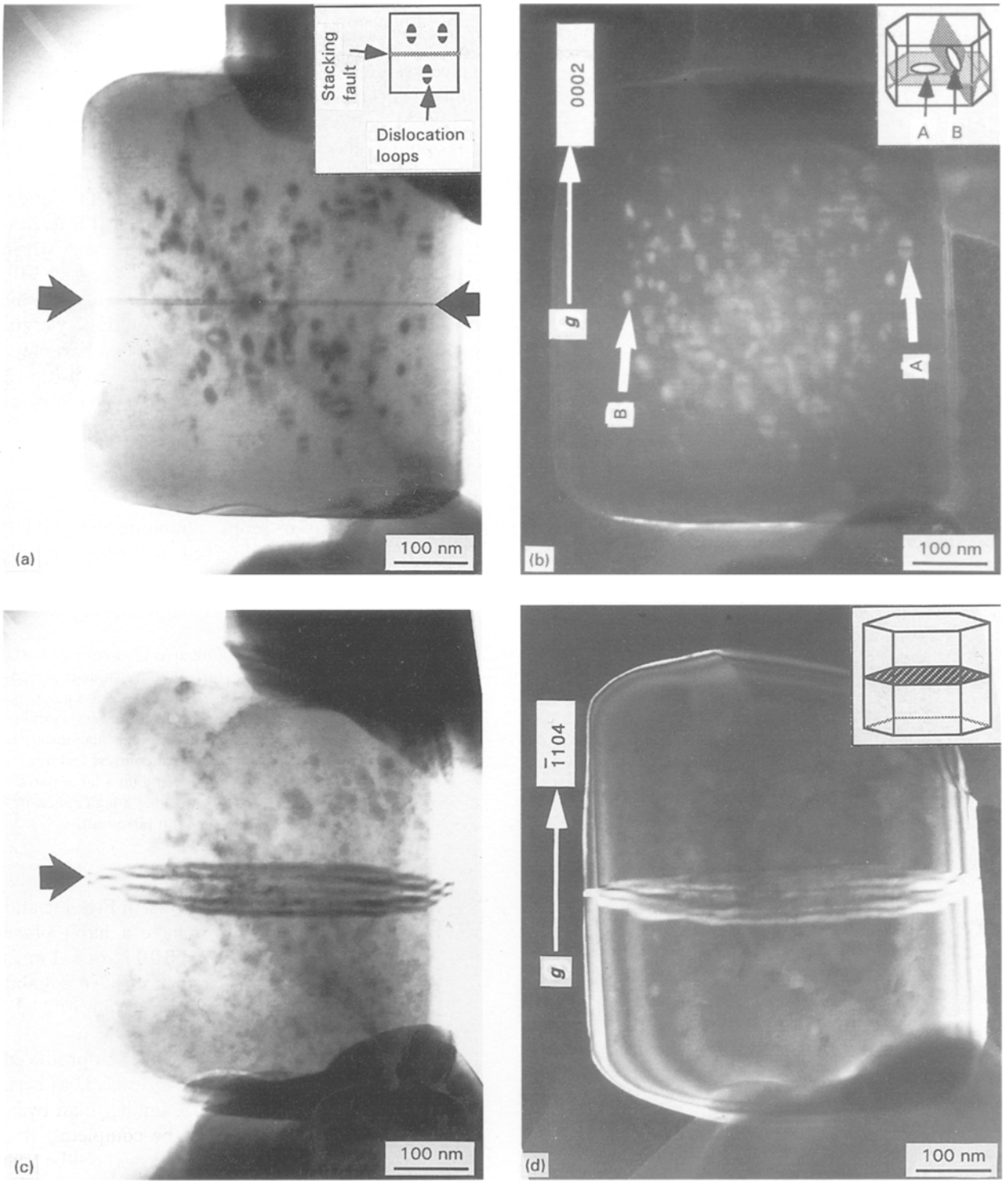

Figure 12 Transmission electron micrographs of typical 1500 °C annealed UBE-E03 silicon nitride powder particle observed from different zone axes, showing the "grown-in" vacancies and their clusters (vacancy-type dislocation loops and the stacking fault), to be a common feature of the powder particles. In (a) bright field and (b) dark field, the zone axis is near $[1\,0\,\bar{1}\,0]$; in (c) bright field and (d) dark field, the zone axis is near $[4\,0\,\bar{4}\,1]$. Loops of type A have the habit plane $\{0\,0\,0\,1\}$ and Burgers vector $(1/n)\langle 0\,0\,0\,1\rangle$ ($n = 1$ or 2); loops of type B have the habit plane $\{\bar{1}\,\bar{1}\,2\,1\}$ and Burgers vector $(1/m)\,\langle 1\,1\,\bar{2}\,3\rangle$ ($m = 3$ or 9) [42, 71, 73].

with a linear dimension of about 10–30 nm are found. Around these centres marked lattice distortion exits, as reflected in the deviation of the $(1\,0\,\bar{1}\,0)$ lattice plane spaces giving measured values ranging from 0.585–0.739 nm, compared with the normal value of 0.677 nm. Concurrently, regions of amorphous phase with a linear dimension of < 10 nm completely enclosed within an otherwise perfect α-silicon nitride lattice, are detected. The amorphous regions were assumed to be the consequence of the electron radiation damage: however, the nature of the strain centres was not specified [74]. Jack [28] has reported the observation of 25 nm intragranular, amorphous, disc-like features in black and white CVD α-silicon nitride (the same materials used by suzuki [47]), which on annealing at 1850 °C coalesced and then disappeared. It was postulated that the discs were precipitates of amorphous silica. Similarly, internal

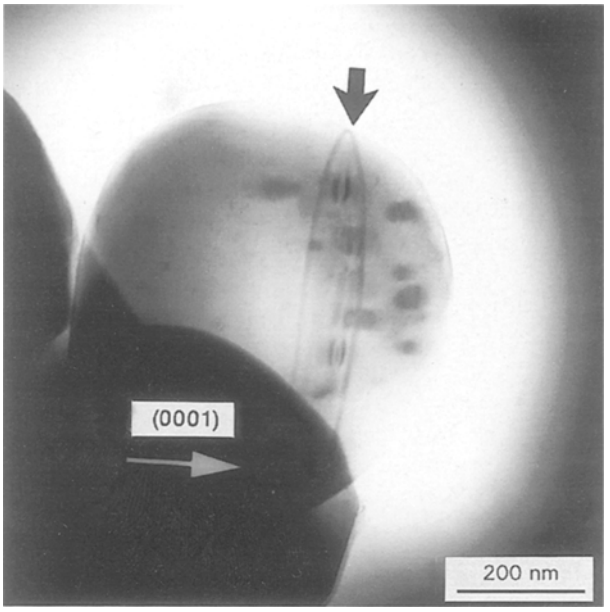

Figure 13 Transmission electron micrograph of UBE-E03 silicon nitride powder particles after annealing at 1750 °C showing the existence of dislocation loops and a stacking fault (arrowed) [42].

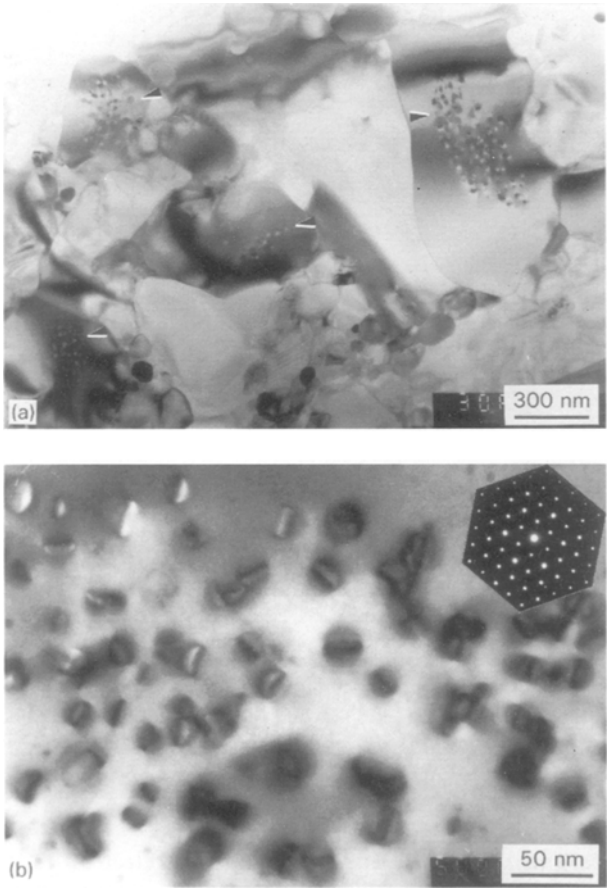

Figure 14 Transmission electron micrographs showing the vacancy-type dislocation loops formed by agglomeration of vacancies in α-silicon nitride grains within bulk materials with $\alpha/\beta = 7/3$ fabricated by hot-pressing a silicon nitride powder (Starck LC12N, produced by the silicon nitridation method) at 1700 °C, and followed by furnace cooling to room temperature: (a) general view and (b) higher magnification. The dislocation loops have a habit plane $\{1\bar{2}10\}$ and Burgers vector $\frac{1}{3}\langle 1\bar{2}10\rangle$ [70].

microstructural features which were assumed to be nano-dimension copper- and tin-rich precipitates have been observed in grains of otherwise high-purity polycrystalline CVD α-silicon nitride. These features similarly disappeared after annealing at 1800 °C [44].

Figs 14 and 15 show typical dislocation loops in a residual α-silicon nitride grain within bulk material fabricated by hot-pressing at 1700 °C a silicon nitride powder which was produced by silicon nitridation, and with a furnace cooling rate. A typical feature is the existence of a dislocation loop-free zone which represents the elastic interaction of a vacancy with a traction-free surface. In Fig. 15 the width of the dislocation loop-free zone around the periphery of the grain is not uniform. This may indicate that part of the boundary is not traction free. Fig. 16 is a high-resolution TEM image of a dislocation loop of a habit plane (0001) and Burgers vector $\frac{1}{2}[0001]$.

3.1.2. β-Silicon nitride

Interstitial dislocation loops inhabiting the $\{10\bar{1}0\}$ planes have been only observed in β-silicon nitride following irradiation [75].

3.2. Planar defects

Both the α-silicon nitride and the β-silicon nitride structures are non-centrosymmetric and therefore

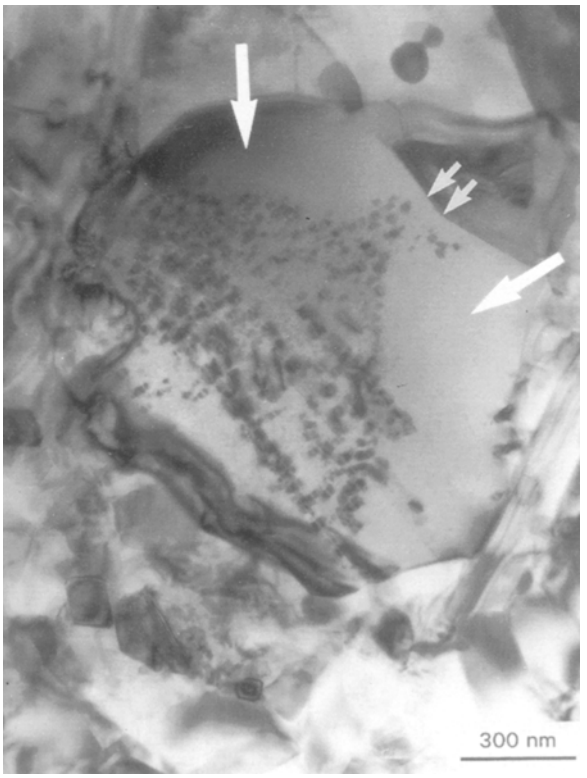

Figure 15 Transmission electron micrographs showing that the distribution of vacancy-type dislocation loops possibly depends on the condition of the grain boundary. It is likely that the double arrowed part of the boundary is not traction free, and hence it is not an effective sink for the vacancies. The part of the boundary adjacent to the dislocation loop-free region (large arrows) is likely to be traction free and hence permits the effective escape of the vacancies.

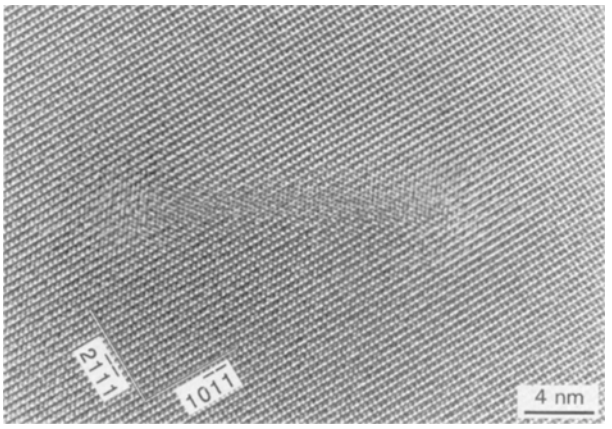

Figure 16 HRTEM image of a loop observed from the zone axis $[\bar{1}\,\bar{3}\,4\,\bar{1}]$. The loop is faulted and has a habit plane (0 0 0 1). The partial dislocation has a Burgers vector of $\frac{1}{2}[0\,0\,0\,1]$.

structurally enantiomorphic domains should exist. Inversion boundaries which separate two domains related by a simple inversion have been demonstrated to exist in the α-silicon nitride structure. The inversion boundaries lie primarily on (0 0 0 1) planes, but they frequently change from one (0 0 0 1) plane to another by going through some irrational planes in between. The configuration, and structural models for the inversion boundaries have been analysed in detail by Hwang and Chen [76].

Other types of structural fault with combinations of rotation and displacement components have also been identified in crystalline α-silicon nitride prepared by the CVD method [77–79]. The faults form extensive facets on basal planes of the α-silicon nitride structure, but also extend on to non-basal planes and curved surfaces within grains. The formation of the faults can be accounted for by the displacement of one stacking layer along the $\langle 1\,\bar{1}\,0\,0\rangle$ direction within the periodic layer stacking ...ABCDABCD....

Several domain boundaries have also been identified in the β-silicon nitride structure [80]. Very well characterized is the domain boundary parallel to the $\{1\,0\,\bar{1}\,0\}$ plane and formed through the relative shear of two identical structural domains with $\frac{1}{6}[\bar{2}\,1\,1\,0]$.

3.3. Linear defects

Previous detailed studies of dislocations in silicon nitride are sparse. For most cases, the presence of dislocations related to densification, grain-boundary phase crystallization, and high-temperature creep processes, are only reported as brief comments [81–83]. Furthermore, far less information is available about dislocations for α-silicon nitride than for β-silicon nitride, as a consequence of the fact that most dense sintered and hot-pressed silicon nitrides are composed of β-silicon nitride grains as a result of the irreversible α- to β-silicon nitride transformation during densification. There may be several reasons why little attention has been directed toward linear defects in silicon nitride. Firstly, it would be expected that, because of the high energies likely to be involved, dislocations would be harder to generate and glide in a covalent material with strong directional inter-atomic bonding, than in predominantly ionic materials, or in metals. Secondly, for a crystal to be able to undergo general homogeneous strain by slip, five independent slip systems are necessary [84]. However, ceramics and especially those with hexagonal symmetry, generally possess few independent slip systems; it is therefore assumed that dislocations do not play an important part in the plastic deformation of silicon nitride. Thirdly, although silicon nitride is expected to be used for high-temperature applications, the unavoidable presence of the intergranular film defines the maximum temperature of use at around 1300 °C, at which dislocations are unlikely to be activated.

The information available about dislocations in silicon nitride is summarized in Table VIII. Evans and Sharp [85], Butler [86], Kossowsky [87], Marquis [88], Lee and Hilmas [89] and Hwang and Chen [76] have analysed the Burgers vectors of dislocations in hot-pressed and reaction-bonded silicon nitride. In both the α-silicon nitride and the β-silicon nitride the most commonly observed dislocations have a $\langle 0\,0\,0\,1\rangle$ type Burgers vector, and the perfect *a*-axis dislocation with Burgers vector $\frac{1}{3}\langle 1\,1\,\bar{2}\,0\rangle$, and the perfect $(a + c)$ axis dislocation with Burgers vector $\frac{1}{3}\langle 1\,1\,\bar{2}\,3\rangle$ are also identified. Fig. 17 shows dislocations with a Burgers vector of [0 0 0 1] in a β-silicon nitride grain within a polycrystalline silicon nitride material hot-pressed at 1700 °C. Consideration of the strain energies associated with various types of dislocation in the β-silicon nitride indicate that $\langle 0\,0\,0\,1\rangle$ is the most stable Burgers vector, and an analysis of dislocation mobility using the Peierls model suggested they would also be the most mobile with $\{1\,0\,\bar{1}\,0\}$ as the primary slip plane and with $\{1\,1\,\bar{2}\,0\}$ and $\{1\,2\,\bar{3}\,0\}$ as the secondary slip planes. Subsequently, indentation data indicated that the slip system identified in β-silicon nitride is also identically applicable to α-silicon nitride. For the primary slip systems, $\langle 0\,0\,0\,1\rangle\{1\,0\,\bar{1}\,0\}$, two are independent and there are three different ways of choosing these.

In α-silicon nitride, the dislocations with the smallest Burgers vectors are the *c*-axis (0.5591 nm) and the *a*-axis (0.7818 nm). It seems then that in an α-silicon nitride *a*- and *c*-axis dislocations should have a similar line energy, and are able to be generated at similar frequencies. In β-silicon nitride, the *c*-axis dislocations have been commonly reported, but *a*-axis dislocations and the mixed dislocations rarely so. This is understandable because in β-silicon nitride the *c*-axis Burgers vector is only 0.2911 nm, while the *a*-axis Burgers vector is 0.7608 nm, making the *a*-axis dislocation energetically unfavourable.

Although α-silicon nitride and β-silicon nitride have the same primary slip system, the *c*-axis dislocation in α-silicon nitride has a much larger Burgers vector than the *c*-axis dislocation in the β-silicon nitride. It is expected, in principle, that α-silicon nitride will have a higher hardness and a lower fracture energy than β-silicon nitride, and experimental observations, in fact, indicate that the Vickers hardness on the basal plane for the β-silicon nitride is 28% smaller than that for the α-silicon nitride [90, 91].

TABLE VIII Dislocations in α- and β-silicon nitride

Type	Burgers vector	Slip plane	Phase	Ref.
Perfect, edge	$\langle 0001 \rangle$	$\{10\bar{1}0\}$	α and β	[81, 83, 85, 87]
Perfect	$\frac{1}{3}\langle 1\bar{2}10 \rangle$	–[a]	α and β	[78, 79, 81, 83, 85, 87]
Perfect	$\frac{1}{3}\langle 1\bar{2}13 \rangle$	–	α and β	[78, 79, 81, 86]

[a] (–) Not known.

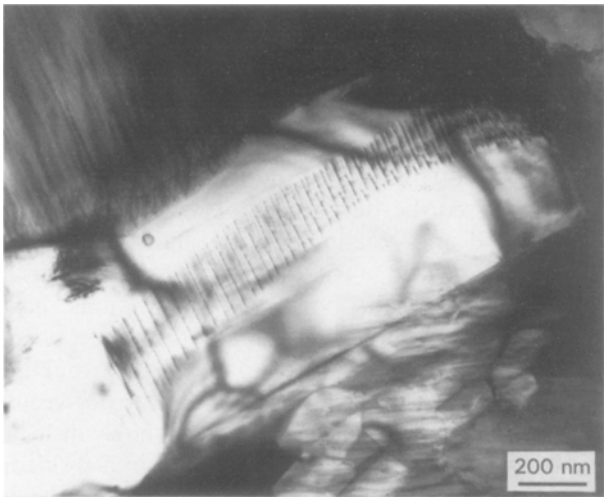

Figure 17 TEM image (bright field) of a group of dislocations with the Burgers vector of $\langle 0001 \rangle$ in a β-silicon nitride grain of as-sintered material.

Kossowsky [68] suggested that dislocation motion in silicon nitride is unlikely to occur at temperatures below 1700 °C. The contribution of dislocation motion to creep can be estimated using the relationship

$$\varepsilon = \rho \boldsymbol{b} x \quad (1)$$

where ε is the plastic strain, ρ the dislocation density, $\boldsymbol{b}$ the value of Burgers vector, and x the average distance moved by a dislocation. For a 1200 °C fatigued silicon nitride, values were set approximately as $\rho = 2 \times 10^{10}\ m^{-2}$, $x = 1\ \mu m$ (grain diameter), and $\boldsymbol{b} = 0.5$ nm, giving a contribution to the measured plastic strain of $< 10^{-5}$. This agrees with the general observation that the creep of liquid-phase sintered silicon nitride is controlled by the intergranular films [67, 68]. Dislocations may well play an active role in high-temperature deformation mechanisms in both monolithic and composite silicon nitride-containing materials. This may be supported by the observation that dislocation motion in reaction-bonded silicon nitride associated with plastic deformation at 1400 °C has been identified [85]. More recently, increased dislocation densities have been reported in materials that had undergone a creep test [89]. However, any possible contributions of dislocation movement to the high-temperature deformation behaviour of silicon nitride is still generally obscured by the behaviour of the intergranular films with respect to firstly limiting the test temperature of the material, and secondly preventing initiation of dislocations within grains by releasing stress concentrations that may be imposed on the grains.

4. Discussion and speculations

As described above, the observation of vacancy clusters in as-grown α-silicon nitride is anomalously high. This involves the very interesting subjects of the origin of the vacancies, and the structural stability of the α-silicon nitride, possibly with respect to oxygen contamination. Thermally activated vacancies of the Schottky and the structural vacancies generated by replacement of nitrogen by oxygen, separately or in combination, may be suggested to contribute to the formation of vacancy clusters in α-silicon nitride.

The concentrations and cluster configurations of the thermally activated vacancies are determined by temperature, sample cooling rate, vacancy formation energy, and vacancy formation kinetics [42].

The consequences of the replacement of nitrogen by oxygen in the α-silicon nitride lattice must be the simultaneous generation of vacancies in both silicon and nitrogen sites to fulfil the electrical neutrality requirement as suggested by Wild *et al.* [9]. Hence, single vacant nitrogen and silicon lattice sites are expected within α-silicon nitride containing structural oxygen. These silicon and nitrogen vacancies have two distinctive features. Firstly, they would be expected to be localized in close proximity to the oxygen atom, hence the mobility of the vacancies and oxygen should then be coupled, and be sensitive to the charge state of the defect, and local defect concentration. As discussed above, the interstices and the interconnecting channels in the α-silicon nitride structure should, in principle, allow the fast diffusion of oxygen atoms (the atomic radius of oxygen is 0.06 nm, compared with the interconnecting channel radius of 0.07 nm). However, simultaneous movements of oxygen and the coupled vacancy at high temperature are believed to be rather difficult owing to the high activation energy involved [28, 44]. Secondly, the vacancy concentration should be determined by the lattice oxygen content. According to Wild *et al.*'s formula [9] of $Si_{11.4}N_{15}O_{0.3}$, 0.9 wt % oxygen is contained in the silicon nitride lattice. Each unit cell ($Si_{12}N_{16}$) on average has 0.6 silicon and 0.7 nitrogen vacancies, equivalent to a Schottky vacancy concentration of 5×10^{-2} (three silicon and four nitrogen vacancies). This is almost two orders of magnitude higher than the estimated vacancy concentration in grains of material hot-pressed at 1700 °C. This may be a further illustration that although most of the α-silicon nitride powders contain ~1–2 wt % oxygen, only a very small proportion is actually incorporated within the α-silicon nitride lattice. Inward diffusion of oxygen from the particle surface oxide layer may be one of the mechanisms for incorporation of the lattice oxygen. However, it is generally believed that dissolution of the lattice oxygen mainly occurs accompanying the formation process of the α-silicon nitride due to the formation kinetics.

It is possible to try to quantify the point defect concentration required for the precipitation of the vacancy dislocation loops, on the basis of the observed distributions of loops in the α-silicon nitride grains of material hot-pressed at 1700 °C. In order to simplify the problem, it is assumed that the condensation of thermally activated point defects ($3V_{Si} + 4V_N$) is solely responsible for the formation of the loops. The volume of the unit cell of α-silicon nitride containing four formula units is 0.293 nm^3 (and assuming that a Si_3N_4 "vacancy" ($V_{Si_3N_4}$) consists of a Schottky type of defect with three silicon ($V_{Si}^{''''}$) and four nitrogen ($V_N^{\cdot\cdot\cdot}$) vacant lattice sites), the mean linear dimension for ($V_{Si_3N_4}$) is ~0.42 nm. This indicates that the average loop disc of approximate diameter ~30 nm and thickness of 0.42 nm should require the condensation of ~3000 ($V_{Si_3N_4}$). Based on Figs 15 and 16, an estimated Schottky defect concentration [$V_{Schottky}$] (where the square brackets are used to indicate a fractional concentration) at 1700 °C, calculated on the basis of the volume of vacancies required to form the number of loops divided by the volume of material in which they were counted, is 8×10^{-4}. Assuming that the vacancies are entirely thermally activated defects and making use of mass, site, and charge balance relationships

$$0 = 3[V_{Si}^{''''}] + 4[V_N^{\cdot\cdot\cdot}] \quad (2)$$

where

$$[V_{Si}^{''''}] = 3[V_{Schottky}] \quad (3)$$

and

$$[V_N^{\cdot\cdot\cdot}] = 4[V_{Schottky}] \quad (4)$$

gives a Schottky equilibrium constant, K_s of

$$K_s = 3^3 4^4 [V_{Schottky}]^7 \quad (5)$$

or

$$K_s = 6912[V_{Schottky}]^7 \quad (6)$$

and $\sim 1 \times 10^{-18}$. On the assumption that precipitation of the loops occurs rapidly after initiation of cooling from 1700 °C, $\Delta E_{Schottky}$ is ~680 kJ mol^{-1} (6.2 eV). This value for the Schottky formation energy is very low, given the strong and directional covalent bonding of silicon nitride. The values of Schottky formation energies in other ceramic materials are of interest in this context [92]. A value for the Schottky formation energy has been calculated for α-Al_2O_3 of 25.2 eV, equivalent to a mean energy per vacancy of 5.0 eV, although the calculated values for individual cation and anion vacancies are very much higher than this. In MgO the corresponding values are 7.5 and 3.8 eV; however, a vacancy pair-binding energy of 2.6 eV is found, so that the effective Schottky formation energy is reduced to 4.9 eV. A comparable interaction energy of about 3 eV would be expected for α-Al_2O_3, but even so the final Schottky formation energy value for α-Al_2O_3 must be at least 20 eV. The α-silicon nitride crystal structure has been assumed to be strained because of constraints imposed on the structure by the linking of the alternate AB and CD Si–N layers, and found, in practice, in the construction of the ball and stick model with a rigid and regular SiN_4 tetrahedra. A low value may, in part, be a result of the strain energy of the α-silicon nitride lattice although the disorder entropy term arising from the seven vacant atomic lattice sites must also be a counter-balancing factor. Furthermore, the experimentally observed vacancies should be the sum of the thermally activated vacancies and those related to the structural lattice oxygen. The above calculation is based on the assumption that the experimentally observed vacancies all come from the thermally activated vacancies, giving a higher Schottky vacancy concentration, hence partly inducing underestimation of the $\Delta E_{Schottky}$. It is clear that much more work needs to be done to resolve the question of the energy value for α-silicon nitride.

On the basis of Figs 15 and 16 showing the absence of loops near the edges of the grains, a very approximate measure of the vacancy diffusion coefficient, D_V, for the slowest species (believed to be nitrogen) can be obtained. A shell of ~50 nm is free of loops and using the "random walk" expression of

$$x = (D_V t)^{1/2} \quad (7)$$

and a value for t of ~100 s gives a mean value for D_V of the order of 2×10^{-18} $m^2 s^{-1}$. Thus, a very approximate estimate can be made for the self-diffusion coefficient for nitrogen, D_N, in the α-silicon nitride grains at the hot-pressing temperature (1700 °C). This can be calculated using the relationship

$$D_N = 4D_V[V_{Si_3N_4}] \quad (8)$$

setting D_V of $\sim 2 \times 10^{-18}$ $m^2 s^{-1}$ and $[V_{Si_3N_4}] = 8 \times 10^{-4}$, to give $D_N \sim 6 \times 10^{-21}$ $m^2 s^{-1}$.

The specific formula for α-silicon nitride with lattice oxygen originally proposed by Wild *et al.* [9] was based on thermodynamic considerations, and observations of nitrogen and oxygen partial pressure as well as structural parameters apparently required for the detection of the α- and β-phases. On the assumption that a wider range of oxygen contents can be accommodated within the α-silicon nitride lattice, a more general formula for this phase would be $Si_{(12-0.25x)}N_{(15-x)}O_x$, in which the oxygen is accommodated entirely in the nitrogen sites as O_N^+, with charge balance being provided by one quarter of the number of the silicon vacancies (V_{Si}^{4-}). Any additional (y) nitrogen vacancies would also be balanced by the appropriate concentration of silicon vacancies ($0.25y$), to give the overall composition $Si_{(12-0.25(x+y))}N_{(15-(x+y))}O_x$, and for which Wild *et al.* have suggested a value of y of approximately 1. It would be assumed that the two types of lattice point defect, V_{Si}^{4-} and O_N^+ would be closely located, or coupled, within the lattice. This proportion of the total silicon vacancy concentration might be expected not to have the same mobility as the normal Schottky type of vacancy, and might not therefore be able to participate fully in the Schottky equilibrium equation, $K_s = [V_{Si}^{4-}]^3[V_N^{3+}]^4$. This discussion of point-defect types and concentration is of necessity highly speculative, because of the almost complete lack of reliable information.

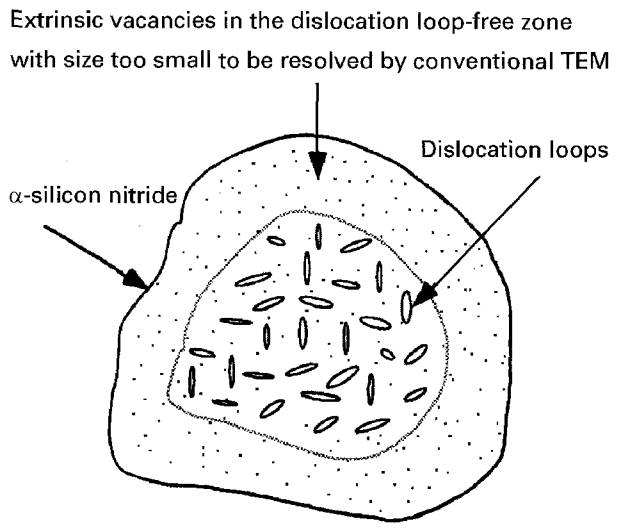

Figure 18 Schematic drawing of the distributions of vacancies and vacancy clusters in association with the extrinsic and intrinsic factors in α-silicon nitride. The extrinsic vacancies are too small to be resolved by conventional TEM within the dislocation loop-free zone [73].

A reasonable speculation, pertinent to the existing experimental observation, may therefore be that the observed strain centres and vacancy clusters within α-silicon nitride are generated by the agglomeration of both types of vacancies, thermally activated and extrinsic. The vacancy concentration, clustering behaviour, and size of the cluster will be determined by a variety of factors and further work is needed to clarify those interrelations. Because of the different mobilities of the two types of vacancies, caution must be taken in interpretation of the distribution of the dislocation loops (the dislocation loop-free zone). Although the resolution limit of TEM to dislocation loops may reach several nanometres, further small vacancy clusters may still exist in the dislocation loop-free zone as schematically shown in Fig. 18 [42].

Two reasons may be suggested why dislocation loops appear to develop only in α-silicon nitride [40]. Firstly, the more stable β-silicon nitride may be unable to generate the required high concentration of Schottky defects, while the more highly strained α-silicon nitride crystals do so in order to release lattice strain energy. Secondly, higher diffusion coefficients in the β-silicon nitride may permit more effectively the escape of vacancies to the grain surface during cooling. Measured values of diffusion coefficients predict that nitrogen tracer diffusion in β-silicon nitride is 10^3–10^4 times faster at 1300 °C than in α-silicon nitride, and therefore vacancies must be expected to be correspondingly more mobile in β-silicon nitride than in α-silicon nitride.

5. Conclusion

Silicon nitride has two polymorphic forms, α-phase and β-phase with the β-phase being thermodynamically more stable at all temperatures. The α-phase is a slightly strained structure, because of constraints imposed by the alternate stacking of the AB and CD Si–N layers. Both the α-phase and β-phase can, in principle, exist as stoichiometric compositions: $Si_{12}N_{16}$ with trigonal symmetry and space group P31*c* for the α-phase; Si_6N_8 with hexagonal symmetry and space group $P6_3$ for the β-phase.

Collectively, the experimental evidence strongly indicates that the formation of the two forms is mainly determined by kinetic factors rather than by thermodynamic ones. Formation of the α-phase silicon nitride may be kinetically favoured by vapour-phase reactions involving the presence of oxygen. The α-phase appears to have the following basic features: firstly, nitrogen can be partially replaced by oxygen, of which the content and distribution are determined by the availability of the oxygen and will depend on the specific production process; secondly, high concentrations of vacancies which are developed in association with the release of the lattice strain energy, and with replacement of nitrogen by oxygen to fulfil the electroneutrality requirements, seem to be a normal structural feature of the phase. Thus the vacancies can be regarded as an extrinsic defect in the as-grown α-silicon nitride. The concentration and configuration of the oxygen and vacancies in α-silicon nitride are therefore likely to be dependent on the specific fabrication process and environment, and the availability of oxygen, reaction rate, annealing time and cooling rate. The β-phase is formed mostly through the involvement of a liquid phase. The α-phase grains may be distinguished from β-phase grains in TEM images by the positive identification of vacancy clusters, which seem to be unique for the α-phase. The wide variation in the unit-cell dimension, and densities, of α-phase silicon nitride is attributable to the differences in concentration and configuration of these lattice defects and lattice oxygen concentrations. With increasing concentration of lattice oxygen in the α-phase, the unit-cell volume decreases. It is possible that the superlattices, nano-cracks, and strain centres earlier claimed to have been detected in α-silicon nitride [51], are related to differences in the configuration of the vacancy clusters.

Any possible contribution of dislocation movement to the high-temperature deformation behaviour of silicon nitride is likely to be masked by the amorphous intergranular films through the release of stress concentrations to prevent initiation and movement of dislocations.

Because α-silicon nitride powder is the basic raw material for several groups of materials encompassing structural and semiconductor applications, the pre-existing vacancies and related defects in α-silicon nitride powder particles must be taken into account in considering the finer details of the microstructural development processes: the α- to β-phase transformation; the formation and defect structure of the α′-sialons; epitaxial grain growth of α′-sialon from α-silicon nitride; the high-temperature mechanical behaviour of α-silicon nitride and its nano-composite. The exact configuration and agglomeration behaviour of vacancies requires detailed study using the positron annihilation method.

Acknowledgements

The authors thank Dr Y. F. Cheng for critical discussion of the presentation of crystal structure data, Dr. H. Gu for drawing attention to some of the literature, and Professor S. L. Wen, Shanghai Institute of Ceramics, for communicating his results about defects in α-silicon nitride. C. M. W. is grateful to the Alexander von Humboldt Foundation for generous financial support through the award of a research fellowship enabling this work to be done.

References

1. J. F. COLLINS and R. W. GERBY, *Metals* **7** (1955) 612.
2. K. H. JACK, *Mater. Res. Soc. Symp. Proc.* **287** (1993) 15.
3. A. M. SAGE and J. H. HISTED, *Powder Metall.* **4** (1961) 196.
4. B. VASSILIOU and F. G. WILDE, *Nature* **179** (1957) 435.
5. P. POPPER and S. N. RUDDLESDEN, *ibid.* **179** (1957) 1129.
6. D. HARDIE and K. H. JACK, *ibid.* **180** (1957) 332.
7. S. N. RUDDLESDEN and P. POPPER, *Acta Crystallogr.* **11** (1958) 465.
8. P. GRIEVESON, K. H. JACK and S. WILDE, "Special Ceramics", edited by P. Popper, **4** (George Faulkner Press, Manchester, 1968) p. 237.
9. S. WILD, P. GRIEVESON and K. H. JACK, *ibid.* **5** (1972) p. 385.
10. D. S. THOMPSON and P. L. PRATT, *Sci. Ceram.* **3** (1967) 33.
11. R. GRÜN, *Acta Crystallogr.* **B35** (1979) 800.
12. P. GOODMAN and M. O'KEEFFE, *ibid.* **B36** (1980) 2891.
13. Y. BANDO, *ibid.* **B39** (1983) 185.
14. O. BORGEN and H. M. SEIP, *Acta Chem. Scand.* **15** (1961) 1789.
15. R. MARCHAND, Y. LAURENT and J. LANG, *Acta Crystallogr.* **B25** (1969) 2157.
16. H. F. PRIEST, F. C. BURNS, G. L. PRIEST and E. C. SKAAR, *J. Am. Ceram. Soc.* **56** (1973) 395.
17. I. KOHATSU and J. W. McCAULEY, *Mater. Res. Bull.* **9** (1974) 917.
18. A. J. EDWARDS, D. P. ELIAS, M. W. LINDLEY, A. ATKINSON and A. J. MOULSON, *J. Mater. Sci.* **9** (1974) 516.
19. K. KIJIMA, K. KATO, Z. INOUE and H. TANAKA, *ibid.* **10** (1975) 362.
20. K. KATO, Z. INOUE, K. KIJIMA, J. KAWADA, H. TANAKA and T. YAMANE, *J. Am. Ceram. Soc.* **58** (1975) 90.
21. K. BLEGEN, "Special Ceramics", edited by P. Popper, Vol. **6** (George Faulkner Press, Manchester, 1975) 223.
22. S. R. SRINIVASA, L. CARTZ, J. D. JORGENSEN, T. G. WORLTO, S. A. BEYERLEIN and M. BILLY, *J. Appl. Crystallogr.* **10** (1977) 146.
23. I. COLQUOHOUN, S. WILDE, P. GRIEVESON and K. H. JACK, *Proc. B. Ceram. Soc.* **22** (1973) 207.
24. H. FELD, P. ETTMAYER and I. PETZENHAUSER, *Ber. Deut. Keram. Ges.* **51** (1974) 127.
25. S. HAMPSHIRE, H. K. PARK, D. P. THOMPSON and K. H. JACK, *Nature* **274** (1978) 800.
26. M. PEUCKERT and P. GREIL, *J. Mater. Sci.* **22** (1987) 3717.
27. G. PETZOW and R. SERSALE, *Pure Appl. Chem.* **59** (1987) 1673.
28. K. H. JACK, in "Progress in Nitrogen ceramics", edited by F. L. Riley (Martinus Nijhoff, The Hague, 1983) p 45.
29. *Idem, J. Mater. Sci.* **11** (1976) 1135.
30. M. H. LEWIS, G. L. WARD and C. JASPER, *Ceram. Trans.* **1B** (1988) 1019.
31. D. R. MESSIER, F. L. RILEY and R. J. BROOK, *J. Mater. Sci.* **13** (1978) 1199.
32. M. J. HOFFMAN and G. PETZOW, *Mater. Res. Soc. Symp. Proc.* **287** (1993) 3.
33. M. MITOMO and Y. TAJIMA, *J. Jpn Ceram. Soc.* **99** (1991) 1015.
34. H. J. KLEEBE, M. K. CINIBULK, R. M. CANNON and M. RÜHLE, *J. Am. Ceram. Soc.* **76** (1993) 1969.
35. T. EKSTRÖM and M. NYGREN, *ibid.* **75** (1992) 259.
36. G. Z. CAO and R. METSELAAR, *Chem. Mater.* **3** (1991) 242.
37. K. HIRAGA, K. TSUNO, D. SHINDO, M. HIRABAYASHI, S. HAYASHI and T. HIRAI, *Philos. Mag.* **A 47** (1983) 483.
38. K. L. MOORE, *Proc. Electron Microsc. Soc. Am.* **49** (1991) 936.
39. H. SUEMATSU, J. J. PETROVIC and T. E. MITCHELL, *ibid.* **50** (1992) 342.
40. C. M. WANG, *Philos. Mag. Lett.* **72** (1995) 111.
41. C. M. WANG and F. L. RILEY, *J. Eur. Ceram. Soc.* **16** (1996) 679.
42. C. M. WANG, X. Q. PAN and M. RÜHLE, *J. Mater. Res.*, **11** (1996) 1682.
43. A. SAWAGUCHI, K. TODA and K. NIIHARA, *J. Am. Ceram. Soc.* **74** (1991) 1142.
44. K. P. KUNZ, V. K. SARIN, R. F. DAVIS and S. R. BRYAN, *Mater. Sci. Eng.* **A105/106** (1988) 47.
45. C. M. B. HENDERSON and D. TAYLOR, *Trans. J. Br. Ceram. Soc.* **74** (1975) 49.
46. W. D. FORGENG and B. F. DECKER, *Trans. Met. Soc. AIME* **212** (1958) 343.
47. H. SUZUKI, *Bull. Tokyo Inst. Technol.* **54** (1963) 163.
48. J. SZEPVÖLGYI, F. L. RILEY, I. MOHAI, I. BERTOTI and E. GILBART, *J. Mater. Chem.* in press.
49. K. OKADA, K. FUKUYAMA and Y. KAMESHIMA, *J. Am. Ceram. Soc.* **78** (1995) 2021.
50. K. NIIHARA and T. HIRAI, *J. Mater. Sci.* **12** (1977) 1233.
51. F. GALASSO, L. KUNTZ and W. J. CROFT, *J. Am. Ceram. Soc.* **55** (1972) 431.
52. K. NIIHARA and T. HIRAI, *J. Mater. Sci.* **14** (1979) 1952.
53. D. P. ELIAS and M. W. LINDLEY, *ibid.* **11** (1976) 1278.
54. A. J. MOULSON, *ibid.* **14** (1979) 1017.
55. M. W. LINDLEY, D. P. ELIAS, B. F. JONES and K. C. PITMAN, *ibid.* **14** (1979) 70.
56. P. LONGLAND and A. J. MOULSON, *ibid.* **13** (1978) 2279.
57. M. MITOMO, *ibid.* **12** (1977) 273.
58. T. NARUSHIMA, N. UEDA, M. TAHEUCHI, F. ISHII and Y. IGUCHI, *Mater. Trans. JIM* **35** (1994) 821.
59. T. HIRAI and S. HAYASHI, *J. Am. Ceram. Soc.* **64** (1981) C88.
60. R. M. LAINE, F. BABONNEAU, K. Y. BLOWHOWIAK, R. A. KENNISH, J. A. RAHN, G. J. EXARHOS and K. WALDNER, *ibid.* **78** (1995) 137.
61. T. YAMADA, T. KAWAHITO and T. IWAI, *J. Mater. Sci. Lett.* **2** (1983) 275.
62. P. DREW and M. H. LEWIS, *J. Mater. Sci.* **9** (1974) 261.
63. H. MANDAL, D. P. THOMPSON and T. EKSTROM, *J. Eur. Ceram. Soc.* **12** (1993) 421.
64. M. KRAMER, M. J. HOFFMANN and G. PETZOW, *Acta Metall. Mater.* **41** (1993) 2939.
65. S. HAMPSHIRE and K. H. JACK, *Proc. Br. Ceram. Soc.* **31** (1981) 37.
66. I. TANAKA, H. J. KLEEBE, M. K. CINIBULK, J. BRULEY, D. R. CLARKE and M. RÜHLE, *J. Am. Ceram. Soc.* **77** (1994) 911.
67. C. J. GASDASKA, *ibid.* **77** (1994) 2408.
68. R. KOSSOWSKY, *ibid.* **56** (1973) 531.
69. H. SCHMID and M. RÜHLE, *J. Mater. Sci.* **19** (1984) 615.
70. C. M. WANG, F. L. RILEY, F. CASTRO and I. ITURRIZA, *J. Am. Ceram. Soc.* **76** (1993) 2136.
71. C. M. WANG, *ibid.* **78** (1995) 3393.
72. C. M. WANG, X. Q. PAN, M. RÜHLE, and F. L. RILEY, *ibid.*, submitted.
73. C. M. WANG, (1996) unpublished work.
74. S. L. WEN and J. W. FENG, *Mater. Lett.* **4** (1986) 420.
75. R. A. YOUNGMAN and T. E. MITCHELL, *Radiat. Eff.* **74** (1983) 267.
76. S. L. HWANG and I. W. CHEN, *J. Am. Ceram. Soc.* **77** (1994) 1711.
77. T. M. SHAW, J. W. STEEDS and D. R. CLARKE, *Mater. Res. Soc. Symp. Proc.* **32** (1984) 325.
78. D. S. ZHOU and T. E. MITCHELL, *Philos. Mag. A* **72** (1995) 1131.
79. D. S. ZHOU and T. E. MITCHELL, *J. Am. Ceram. Soc.* **78** (1995) 3133.
80. H. HIRAGA, M. HIRABAYASHI, S. HAYASHI and T. HIRAI, *ibid.* **66** (1983) 539.

81. K. NUTTAL and D. P. THOMPSON, *J. Mater. Sci.* **9** (1974) 850.
82. S. L. HWANG and I. W. CHEN, *J. Am. Ceram. Soc.* **77** (1994) 2575.
83. *Idem, ibid.* **77** (1994) 1719.
84. G. W. GROVES and A. KELLY, *Philos. Mag.* **8** (1963) 877.
85. A. G. EVANS and J. V. SHARP, *J. Mater. Sci.* **6** (1971) 1292.
86. E. BUTLER, *Philos. Mag.* **21** (1971) 829.
87. R. KOSSOWSKY, *J. Mater. Sci.* **8** (1973) 1603.
88. P. M. MARQUIS, *ibid.* **12** (1977) 424.
89. W. E. LEE and G. E. HILMAS, *J. Am. Ceram. Soc.* **72** (1989) 1931.
90. D. CHAKRABORTY and J. MUKERJI, *J. Mater. Sci.* **15** (1980) 3051.
91. K. NIIHARA and T. HIRAI, *ibid.* **13** (1978) 2278.
92. W. C. MACKRODT, in "Structures and properties of MgO and Al_2O_3 ceramics", edited by W. D. Kingery, "Advances in Ceramics", **10** (The American Ceramic Society, Columbus, OH, 1984) p. 62.

Received 12 June 1995
and accepted 20 February 1996